Dalton Transactions

ROYAL SOCIETY OF CHEMISTRY

PAPER

View Article Online
View Journal | View Issue

Cite this: *Dalton Trans.*, 2025, **54**, 15432

Lanthanide complexes bearing a bioinspired Cu^{II} binding site with picomolar affinity: synthesis, structural, relaxometric and luminescence studies

Katharina Zimmeter,[a] Bertrand Vileno,[a] Agnès Pallier,[b] Carlos Platas-Iglesias,[c] Peter Faller,[a,d] Célia S. Bonnet*[b] and Angélique Sour*[a]

In the pursuit of Cu^{II}-responsive MRI contrast agents with enhanced Cu^{II} affinity, we report the synthesis and characterization of two Ln^{III}-DO3A-C3AmpicGH complexes (Ln^{III} = Gd^{III}, Eu^{III}), featuring a tetradentate Cu^{II}-binding moiety, along with the corresponding mononuclear Cu^{II}-C3AmpicGH complex. The chelator coordinates Cu^{II} through two amide groups, a pyridine and an imidazole ring. The use of a propyl-amide linker between the Ln^{III}- and Cu^{II}-binding moieties allowed an increased separation between the two metal centers. As a result, both Ln^{III}–Cu^{II}-DO3A-C3AmpicGH and Cu^{II}-C3AmpicGH complexes exhibit the same Cu^{II}-affinity ($\log K$ = 11–12 at pH 7.4) and good selectivity over competing physiological metal ions, particularly Zn^{II} (up to at least 500 equivalents). While the Gd^{III} complex displayed no relaxivity changes upon Cu^{II} binding, the Eu^{III} analogue showed a luminescence turn-off response. Spectroscopic analyses as well as density functional theory (DFT) calculations provide insights into the coordination environments of both metal ions, notably confirming the absence of amide coordination to the Ln^{III} center, even in absence of Cu^{II}.

Received 23rd July 2025,
Accepted 22nd September 2025

DOI: 10.1039/d5dt01735a

rsc.li/dalton

1. Introduction

Copper is an essential trace metal ion, required for various physiological processes in the human body, such as electron transfer and redox catalysis.[1,2] An imbalance in copper ions—whether an excess or a deficiency—has been linked to various diseases, highlighting the critical importance of precisely regulating copper homeostasis in the body. In the extracellular medium, Cu ions are mainly in the oxidized Cu^{II} state and are never found as "free ions", but are always bound to a carrier, which can be a protein, peptide or small molecule. Depending on the nature of the complex, this binding is either kinetically inert, such as Cu bound to the ferroxidase ceruloplasmin in the blood,[3] or more labile, forming the "exchangeable copper (Cu_{exc}) pool". Cu_{exc} is mainly bound to human serum albumin (HSA) in the blood, with an conditional association constant of $\log K_a$ = 13 at pH 7.4.[4,5] The exchangeable Cu pool is also present in extracellular fluids of the brain, particularly in the case of certain diseases. Cu^{II} can be bound to amyloid beta (Aβ) peptides with picomolar affinities ($\log K_a$ = 10 at pH 7.4 for $A\beta_{1-16}$) in the case of Alzheimer's disease (AD).[6–8] In the case of Parkinson's disease, Cu is considered to bind to the protein alpha synuclein (α-Syn), although this interaction is still discussed. In test tubes, experiments revealed two distinct Cu^{II} sites in α-Syn with nM and μM affinities respectively (site 1: α-Syn_{1-17}: $K_a = 0.94 \times 10^{-9}$, site 2: α-$Syn_{46-50}$: $K_a = 1.5 \times 10^{-6}$).[9–11]

It has been shown that the quantification of exchangeable copper in the blood has clinical significance for the diagnosis of Wilson's disease and a type of AD.[12–14] Monitoring this Cu^{II} pool could also bring important information for a better understanding of the Cu metabolism. Consequently, the development of Cu-responsive sensors associated to imaging modalities has attracted significant attention. In the literature, Cu^{II}-responsive sensors reported so far rely on luminescence-based techniques, mostly involving quenching of the emission intensity upon interaction with paramagnetic Cu^{II} ions. In contrast, only a few examples are reported with the use of magnetic resonance imaging (MRI) as a detection method.[15,16]

MRI is a powerful technique that provides images with no depth limitation, high spatial resolution and allows real-time monitoring of dynamic processes. Contrast agents (CAs) based on gadolinium(III) complexes are commonly used to enhance image contrast. Upon interaction of the Gd^{III} ion with surrounding water molecules, the relaxation rate of water protons is increased, resulting in an improved contrast. Relaxivity values define the efficiency of a CA to increase the relaxation

[a]*Institut de Chimie (UMR 7177), Université de Strasbourg – CNRS, 4 Rue Blaise Pascal, 67070 Strasbourg, France. E-mail: a.sour@unistra.fr*
[b]*Centre de Biophysique Moléculaire, CNRS, Université d'Orléans, Rue Charles Sadron, 45071 Orléans, France. E-mail: celia.bonnet@cnrs-orleans.fr*
[c]*Departamento de Química Fundamental, Universidade da Coruña, Campus da Zapateira, Rúa da Fraga 10, 15008 A Coruña, Spain*
[d]*Institut Universitaire de France (IUF), 1 rue Descartes, 75231 Paris, France*

rate (r_1 for the longitudinal relaxation rate) of surrounding water protons.[17–19] Cation-responsive CAs can be rationally engineered through the incorporation of an ion-binding site, and the change in relaxivity upon cation binding should be significantly pronounced to enable the detection of cations at low concentrations. This is generally achieved through a change in the number of Gd^{III}-bound water molecules q and/or through a modification of the rotational correlation time τ_R of the complex upon cation interaction.[16,20–24]

Besides the relaxivity change upon metal binding, the CA should present an affinity tuned to that of the physiological Cu_{exc} pool and its surrounding biochemical environment. This affinity should be sufficient to enable competitive extraction of Cu^{II} from its carrier, but not too strong to avoid Cu^{II} depletion. Typically, the CA should be able to retrieve Cu^{II} bound to HSA in the blood, or bound to Aβ- or α-Syn in the brain. Moreover, the CA should also show good selectivity for Cu^{II} over other metal ions, notably over zinc, more abundant in the body and more readily available.[25–27] Finally, the kinetics of Cu^{II} capture and release should ideally match the temporal window of MRI acquisition, although achieving precise control over this parameter remains a challenge.

Fulfilling all these requirements is a real challenge, and since the first example of Cu^{II}-responsive CA was reported nearly twenty years ago,[28] none of the complexes developed fulfill all the criteria. It should be however noted that one Gd^{III} complex based on a τ_R change through an interaction with human serum albumin (HSA) was successfully used to detect Cu^{II} in the liver,[29] although the selectivity *vs.* Zn^{II} is not ideal.

In order to attain high relaxivity changes, a change in the hydration number of Gd^{III} from 0 to 2 is highly desirable. We have previously developed a series of Gd-DO3A-based complexes linked to a pyridine-based switching arm, bearing a Cu^{II} binding site bioinspired by the N-terminal Cu^{II} binding motif of HSA (ATCUN).[30,31] An unprecedented relaxivity increase of *ca.* 400% could be achieved with the compound Gd-DO3A-pyrGH (Fig. 1).[30] Importantly, due to its bioinspired nature, this system is highly selective for Cu^{II} over Zn^{II}. Unfortunately, the Cu^{II} affinity of the bioinspired binding site is drastically reduced when it is tethered to the Gd^{III} complex, with an apparent binding constant (at pH 7.4) dropping from $\log K_{app}$ = 16 for the free binding site to $\log K_{app}$ = 5.6 in the conjugated system.[30,32] This is explained by the distortion of the Cu^{II} coordination sphere due to the proximity of the bulky GdDO3A moiety, along with possible electrostatic repulsion between Cu^{II} and Gd^{III} ions and by the energy cost to switch the pyridine moiety from Gd^{III} to Cu^{II}.

Therefore, one route to increase the affinity of the Gd^{III}-based sensor for Cu^{II} is to increase the distance between the Gd^{III} and Cu^{II} complexing moieties. Alkyl-amide groups have already been successfully used for Zn^{II} and Ca^{II} detection, triggering an increase in the hydration number of the Ln^{III} upon cation binding.[33–35] It has been shown that the length of the linker, ethyl or propyl, plays a crucial role in the hydration number of the Ln^{III} ion, being 1 and 0, respectively.[35,36] For the propyl linker, the overall charge of the complex,[37,38] as well as the steric hindrance of the group linked to the amide function are also important.[39]

This has prompted us to design Gd^{III}-DO3A-C3AmpicH (Scheme 1) containing a Gd-DO3A subunit (DO3A: 1,4,7,10-tetraazacyclododecane-1,4,7-triacetate), a bioinspired Cu^{II} binding site, and a propyl amide function between the two. The bioinspired Cu^{II} binding site C3AmpicH is derived from previously studied ligands which are inspired by the ATCUN site of HSA, and which show ideal Cu^{II} affinity and selectivity *versus* Zn^{II}.[4,26,40] Here, we describe the synthesis of the compounds C3AmpicH and Ln^{III}-DO3A-C3AmpicH, and we evaluate their properties by spectroscopy, relaxivity, and DFT calculations, both in the absence and in the presence of Cu^{II}.

2. Results and discussion

2.1 Design and synthesis of DO3A-C3AmpicH and C3AmpicH

The ditopic ligand was obtained using a combination of solution and solid phase synthesis (SPS), as shown in Scheme 2. The DO3A subunit was linked to a protected 3-bromopropylamine chain **1** to give the protected compound **2**. Deprotection of the amine under basic conditions afforded compound **3**, which was then coupled with the monoactivated pyridine-2,6-dicarboxylic acid. The resulting compound **4** was then linked to a trityl (Trt)-protected histidine (His) residue on a Rink

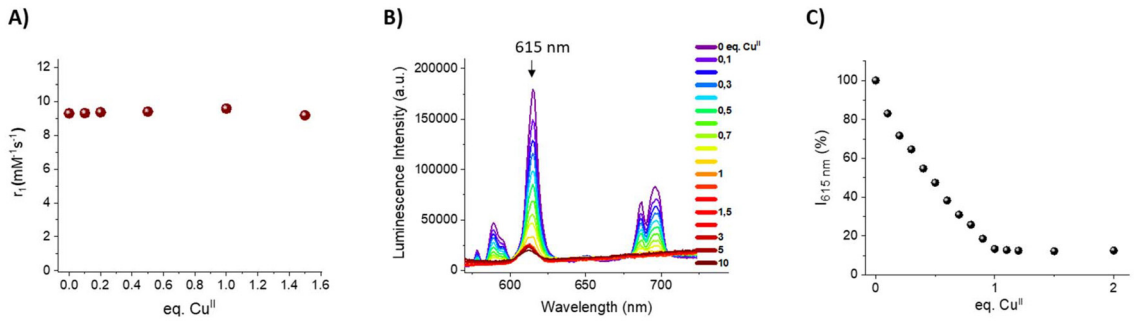

Fig. 1 (A) Relaxivity (r_1, 60 MHz, 25 °C) of Gd^{III}-DO3A-C3AmpicH upon addition of $CuCl_2$. Conditions: 1.68 mM Gd^{III}-DO3A-C3AmpicH, 100 mM HEPES buffer pH 7.4. (B) Luminescence of Eu^{III}-DO3A-C3AmpicH upon addition of $CuCl_2$. Conditions: 60 μM Eu^{III}-DO3A-C3AmpicH, 25 mM HEPES pH 7.4, addition of $CuCl_2$, λ_{exc} = 277 nm. (C) Decrease of the luminescence observed at 615 nm upon addition of $CuCl_2$.

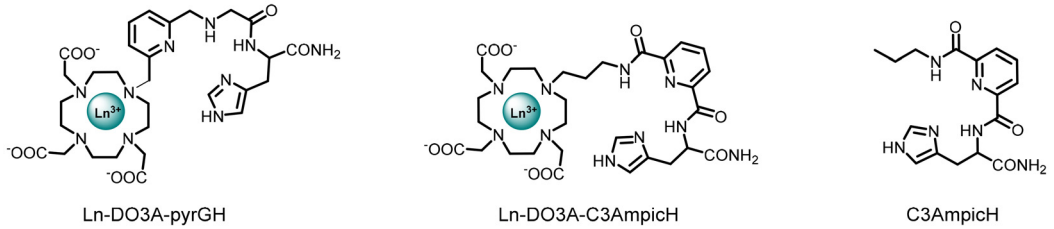

Scheme 1 Chemical structure of the previously studied sensor Ln-DO3A-pyrGH, the new complexes Ln-DO3A-C3AmpicH (with Ln = Gd^{III}, Eu^{III}) and the Cu^{II}-binding ligand C3AmpicH.

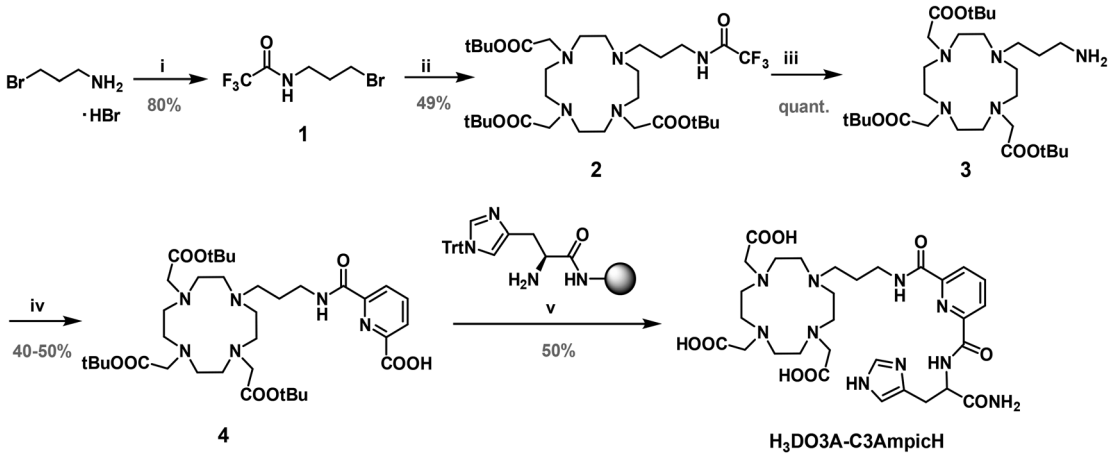

Scheme 2 Synthesis of H_3DO3A-C3AmpicH. Conditions: (i) 1.1 eq. ethyl trifluoroacetate, 1.1 eq. TEA, DCM, rt, 20 h; (ii) 0.83 eq. DO3A*t*Bu, 2.5 eq. K_2CO_3, acetonitrile, 70 °C, 24 h; (iii) 2 eq. aqueous NaOH (0.3 M), EtOH, rt, 5 h; (iv) 4 eq. pyridine-2,6 dicarboxylic acid, 2 eq. DIC, 2 eq. Oxyma Pure, DMF, rt, 3 days; (v) (1) twice: 3 eq. compound **4**, 1 eq. His(Trt)-resin, 2.6 eq. HATU, 6 eq. DIEA, DMF, 2 × 24 h. (2) TFA/TIS/H_2O (95/2.5/2.5) 3 × 30 min. The grey sphere symbolises the Rink Amide resin.

amide resin and the ligand H_3DO3A-C3AmpicH was obtained after deprotection and cleavage from the resin.

The Cu^{II}-binding ligand C3AmpicH was obtained by SPS on a Rink amide resin (section 1 of the SI). The His(Trt) residue was first attached to the resin, followed by the coupling of the monoactivated pyridine-2,6-dicarboxylic acid. The second carboxylic group was activated directly on the resin and coupled to propylamine and the ligand C3AmpicH was obtained after cleavage from the resin and removal of the trityl protecting group.

The final ligands were purified by preparative HPLC and characterized by 1D and 2D NMR and HR-ESI-MS (section 1 of the SI).

2.2 Relaxivity and luminescence responses of Gd^{III}/Eu^{III}-DO3A-C3AmpicH to Cu^{II}

The detection of Cu^{II} by Gd^{III}-DO3A-C3AmpicH has been explored by relaxivity (r_1) measurements in HEPES buffer (pH 7.4) at 60 MHz. As evidenced in Fig. 1A, no relaxivity change upon Cu^{II} coordination is observed. This can be explained by the absence of amide coordination to Gd^{III} even in absence of Cu^{II}, which is in line with the high relaxivity values, and the DFT calculations (*vide infra*).

The Eu^{III} analogue Eu^{III}-DO3A-C3AmpicH was also used to follow Cu^{II} binding by luminescence (Fig. 1B and C). It is well-known that a pyridine can sensitize Eu^{III} luminescence[41,42] and indeed, despite the distance between the Eu^{III} ion and the pyridine moiety, it is also the case here. In the absence of Cu^{II}, the characteristic pattern of Eu^{III} luminescence with emission maxima at 588 nm, 615 nm, 687 nm and 695 nm was observed. Upon addition of Cu^{II}, a linear luminescence decrease was observed and the complete quenching was obtained at a molar ratio of 1 : 1 (Cu : ligand). This turn-off luminescence response evidences Cu^{II} coordination to the Ln^{III} complex. The sharp inflection point observed at 1 equiv. of added Cu^{II} indicates a strong binding.

In order to understand this behavior, we investigated the Cu^{II} coordination mode, as well as the Ln^{III} coordination sphere, both in the absence and presence of Cu^{II}, using electron paramagnetic resonance (EPR), luminescence and relaxivity measurements complemented by DFT calculations.

2.3 Ln^{III}-coordination mode in the complexes Ln^{III}-DO3A-C3AmpicH

First, the structure of Ln^{III}-DO3A-C3AmpicH was investigated. Luminescence lifetime measurements were performed on

Eu^{III}-DO3A-C3AmpicH in H_2O and D_2O to assess the hydration state of the Ln^{III} ion (Table S1 and Fig. S15). In H_2O, the luminescence decays were best fitted by bi-exponential decay pointing to the presence of at least two species in solution with q = 0.1 and 1.7. The apparent predominance of the low-hydration species is however amplified, as the luminescence signal is weighted by the quantum yield of each species. The value of 1.7 is close to that of Eu-DO3A (q = 1.9) where the existence of an equilibrium strongly shifted towards the bis-hydrated species has been evidenced using temperature-dependent UV-Vis spectrophotometry.[43] We certainly have the same phenomenon for Eu^{III}-DO3A-C3AmpicH, which would be consistent with the relaxivity values observed (*vide infra*), and DFT calculations (*vide infra*).

The NMR spectra of the corresponding diamagnetic Y^{III} complex (Fig. S16) supports: (1) the presence of two species in solution in slow equilibrium at the NMR time scale in a ratio 85 : 15; and (2) the lack of coordination of the amide group to Y^{III} as only broad signals for the macrocycle are observed, a fluxional behavior that is characteristic of complexes with flexible DO3A-type ligands. Altogether, this shows that there are several species in solution and the main species is bis-hydrated with no amide coordination.

This is also supported by DFT calculations (Fig. 2), which were used to model the mono-hydrated structure of the complex with the amide group coordinated to the metal ion. Subsequently, we explored the potential energy surface by increasing the $Gd–O_{amide}$ distance, which generated a second energy minimum. Compared to the monohydrated Ln^{III} structure with amide coordination, a difference of free energy of +7.9 kJ mol^{-1} is found. Inspection of the calculated structures shows that the angle formed between the planes of the pyridyl and amide groups increases from 33° to 43° upon amide coordination. Typically, aromatic secondary amides are bent out of the plane of aromatic unit by ~30°, and thus amide coordination appears to be hindered by the presence of the pyridyl-amide group in the vicinity of the DO3A unit.[44] Moreover, the inspection of the enthalpy and entropy contributions obtained with DFT shows that at 298 K the coordination of the amide group is disfavoured by an important entropy contribution of $-T\Delta S$ = 12.8 kJ mol^{-1}, which compensates the negative enthalpy contribution associated to amide coordination (ΔH = −4.9 kJ mol^{-1}). Thus, amide coordination appears to be prevented by the loss of conformational entropy if it binds to the Ln ion.

This is surprising, as it contrasts with previous observations for a Ln^{III}-DO3A complex bearing a propylamide arm linked to a pyridine, which was found to be non-hydrated.[36] This is also in contrast with many propylamide systems developed so far that are either mono or non-hydrated. In our case, the amide is part of an extended aromatic system with a second amide substituted to the pyridine, which probably leads to increased steric hindrance, as reflected in the increase upon amide coordination of the dihedral angle involving the secondary amide and the plane of the pyridyl ring; loss of electronic effects, and rigidity. It shows that the steric hindrance, which remains difficult to evaluate, is important.

The nuclear magnetic resonance dispersion (NMRD) profiles of the corresponding Gd^{III} complex were recorded at pH 7.3 (in HEPES buffer) between 40 kHz and 400 MHz at 25 °C and 37 °C (Fig. 2). As expected for small molecular complexes, the relaxivity decreases with increasing temperature. At 25 °C, 60 MHz, the relaxivity is quite high (r_1 = 9.26 mM^{-1} s^{-1}), which is consistent with a DO3A-type Gd^{III} complex bearing two water molecules in the first coordination sphere.

The NMRD profiles were fitted to the Solomon Bloembergen and Morgan theory to gain access to the microscopic parameters of the complex that affect the observed relaxivity (see SI for equations and details). The values of the water exchange rate, its activation energy and the hydration

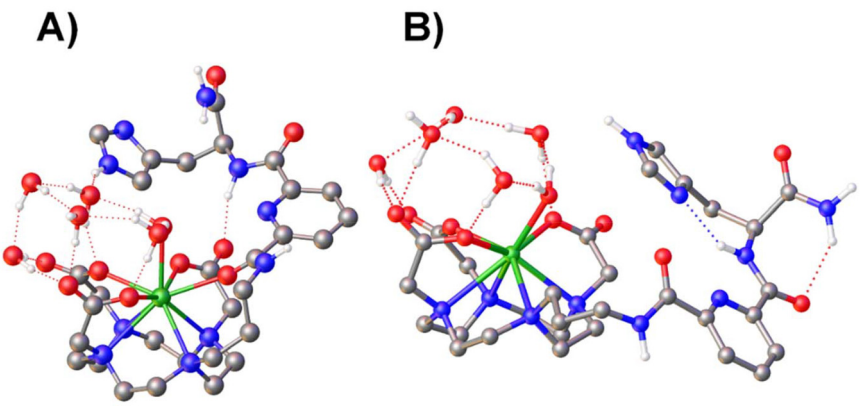

Fig. 2 (A) DFT structure of the monohydrated Eu^{III}-DO3A-C3AmpicH systems showing that amide coordination requires a significant bent of the pyridyl and amide groups, reflected by a O–C–C–N dihedral angle of 44°. The model includes six explicit second-sphere water molecules and a coordinated water molecule. Average bond distances: $Gd–N_{Amine}$ = 2.781 Å; $Gd–O_{Carboxylate}$ = 2.400 Å; $Gd–O_{Amide}$ = 2.427 Å and $Gd–O_{Water}$ = 2.548 Å. (B) Corresponding minimum energy structure obtained upon enlarging the $Gd–O_{Amide}$ bond, providing average bond distances of: $Gd–N_{Amine}$ = 2.698 Å; $Gd–O_{Carboxylate}$ = 2.357 Å; $Gd–O_{Water}$ = 2.481 Å.

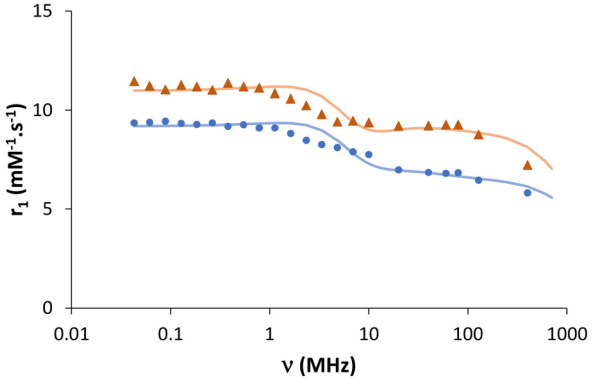

Fig. 3 ^{1}H NMRD profiles of Gd-DO3A-C3AmpicH (1.68 mM) at pH 7.3 (HEPES 0.1 M) at 37 °C (●), and 25 °C (▲). The curves represent the best fit to the SBM theory with the parameters presented in Table S2.

number (q = 1.9) were set to those of GdDO3A[43] due to the similar coordination sphere. Fig. 3 shows the experimental data and the best-fit curves, the parameters of which are reported in Table S2. The rotational correlation time was determined to be 122 ps, which is consistent with the size of the complex. We also checked that the decrease of the hydration number from 1.9 to 1.7 did not affect significantly the rotational correlation time.

2.4 Cu^{II}-coordination mode in the complexes Eu^{III}–Cu^{II}-DO3A-C3AmpicH and Cu^{II}-C3AmpicH

The Cu^{II} coordination sphere was determined in both Cu-C3AmpicH and Eu–Cu-DO3A-C3AmpicH complexes. The Cu^{II} titrations were performed in HEPES buffer at pH 7.4 and followed by UV-visible spectroscopy (Fig. S17 and S19). Upon Cu^{II} addition, a broad d–d absorption band appeared, centered at 595 and 600 nm for Eu–Cu-DO3A-C3AmpicH and Cu-C3AmpicH, respectively. This indicates the formation of a 1 : 1 Cu : ligand complex, which is in accordance with luminescence titrations (Fig. 1B).

It is noteworthy that the d–d bands are more red-shifted than expected for the coordination to two amidates and two aromatic sp^2 nitrogen atoms.[45] Thus, we investigated the pH dependence of the Cu^{II}-coordination sphere of Eu^{III}–Cu^{II}-DO3A-C3AmpicH and Cu^{II}-C3AmpicH by UV-Vis absorption spectroscopy and EPR. A hypsochromic shift of the absorption maximum of the d–d band was observed for both Cu^{II}-complexes from 630 nm (at pH below 6) to 580 nm (at pH above pH 8) (Fig. 4A and S20, S21). This shift can be attributed to a change in the coordination of Cu^{II} due to the deprotonation of the terminal amide when increasing the pH. Such pH-dependent behavior has previously been reported in the literature.[46] At pH below 6, the Cu^{II} ion is linked to the oxygen of the terminal amide, then upon increasing the pH, the amidate is gradually formed and the Cu^{II} ion binds to the nitrogen of the amidate. At pH 7.4, both coordination modes are simultaneously present in solution, in line with a broad d–d band around 600 nm.

To strengthen this hypothesis, low-temperature (100 K) EPR characterization of these complexes was performed at pH 7.0 and 9.4 (Fig. 4B and Table 1). EPR spectra evidenced the presence of two different coordination modes at pH 7.0 and 9.4, in line with a change from a neutral O to a negatively charged N. At this low temperature one coordination mode only is seen at each pH. At pH 7.0, the EPR spectrum suggests a Cu^{II}-coordination sphere composed of three nitrogens and one oxygen atom, and at pH 9.4, a 4N binding mode is highly probable. This is consistent with the UV-Vis absorption data (Fig. 4A), although the pH range in which the coordination change occurs was shifted, which may be due to the temperature difference between the two techniques. The g-tensors observed for the two species ($g_\parallel > g_\perp$; $g_\perp > 2.035$) are characteristic of square-planar coordination with a $d_{x^2-y^2}$ ground state.[47]

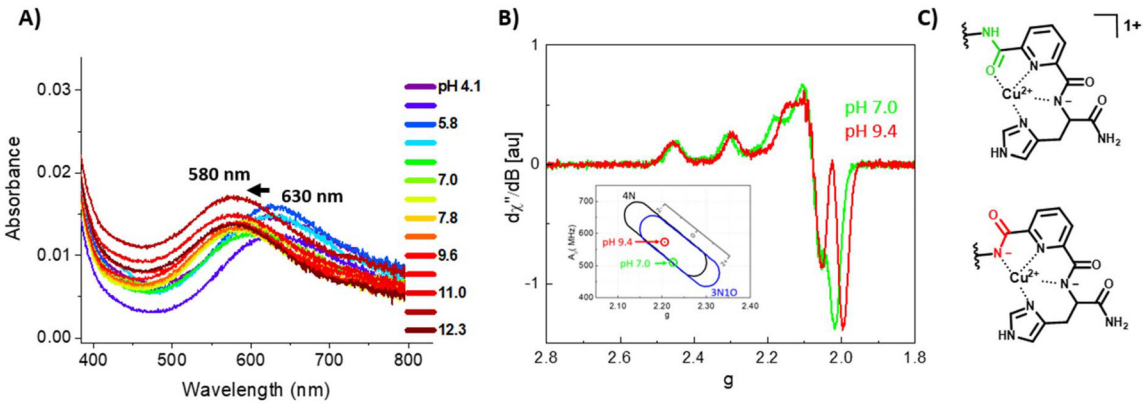

Fig. 4 pH-dependence of the Cu^{II}-binding to Eu^{III}-DO3A-C3AmpicH. (A) UV-Vis: hypsochromic shift of the absorption maximum of the d–d band upon basification. Conditions: 100 μM Eu^{III}-DO3A-C3AmpicH, 90 μM $CuCl_2$, in H_2O, addition of aqueous NaOH, room temperature. (B) EPR: conditions 600 μM Eu^{III}-DO3A-C3AmpicH, 500 μM $CuCl_2$, 75 mM HEPES pH 7.4 or CHES pH 10, 10% glycerol, 100 K. The indicated pH values have been measured on the pH-meter after the addition of glycerol and thus differ slightly from the pH values of the used buffer solutions. Inset: Peisach–Blumberg plot indicating the Cu^{II}-complex coordination sphere as a function of the values of $A_\parallel$and $g_\parallel$ as well as the overall charge of the molecule.[48] (C) Structures showing the proposed Cu^{II}-coordination modes.

Table 1 EPR spectral parameters obtained with DFT calculations for the Cu^{II}-C3AmpicH system[a]

Coordination		$g_{\parallel}$	$g_{\perp}$	$A_{\parallel}$/MHz	$A_{\perp}$/MHz	$g_{\parallel}/A_{\parallel}$/cm
4N	DFT	2.180	2.050	578[b]	28[b]	113
	Exp	2.203		590		112
3N1O	DFT	2.194	2.054	526[b]	37	125
	Exp	2.230		510		131

[a] *g*- and *A*-tensors were calculated using the PBE0-DH and TPSS functionals, respectively (see SI for details). [b] Calculated as negative values.

To further support this pH-dependent coordination mode, DFT calculations were performed for the Cu^{II}-C3AmpicH complex and the resulting structures are shown in Fig. S22. The EPR parameters obtained are in reasonable agreement with the experimental data, in particular when considering the difficulties associated to the calculation of EPR parameters in Cu^{II} complexes (Table 1 and Table S3).[49,50] In particular, the deprotonation in the complex results in a 4N coordination environment that is characterized by a higher $A_{\parallel}$ and a lower $g_{\parallel}$ value than those obtained for the complex with 3N1O coordination (Table 1). This is in line with the changes expected for these coordination environments according to Peisach, as 3N1O coordination is generally characterized by higher $g_{\parallel}$ and lower $A_{\parallel}$ values than 4N coordination, an effect that is magnified by the increased positive charge of the 3N1O complex. We note that the experimental values of $g_{\parallel}/A_{\parallel}$, which are diagnostic of the coordination environment, show a very nice agreement with the DFT values (Table 1).

2.5 Estimation of the Cu^{II}-affinity of Eu^{III}-DO3A-C3AmpicH and C3AmpicH

The affinity of Eu^{III}-DO3A-C3AmpicH and C3Ampyr for Cu^{II} was evaluated by competition experiments with protein or peptides of biological relevance (HSA, $A\beta_{1-16}$ and α-Syn_{1-6}). These competition experiments were followed by UV-Vis absorption, circular dichroism and luminescence spectroscopies.

The competition experiments between Eu^{III}-DO3A-C3AmpicH and HSA for Cu^{II}, were first followed by UV-vis absorption experiments, monitoring the d–d bands of the Cu^{II} complexes. Measurements were performed both by addition of Eu^{III}-DO3A-C3AmpicH to the equimolar Cu^{II}-HSA complex and by addition of the complex Eu^{III}–Cu^{II}-DO3A-C3AmpicH to equimolar HSA (Fig. 5A and S23). Both Cu^{II} exchange reactions lead to the same end-point with a maximum absorbance at 535 nm, suggesting the coexistence of the complexes Cu^{II}-HSA (d–d band maximum at 530 nm) and Eu^{III}–Cu^{II}-DO3A-C3AmpicH (d–d band maximum at 595 nm) at the equilibrium state. This also indicates that only a small fraction of Cu^{II} could be retrieved from HSA, which is in coherence with circular dichroism experiments (Fig. S24). Similar results were obtained with Cu-C3AmPicH (Fig. S25).

The Cu^{II}-affinity of Eu^{III}-DO3A-C3AmpicH and C3AmpicH was further investigated using other physiological ligands with weaker Cu^{II}-affinity, like $A\beta_{1-16}$ ($\log K_a$ = 10)[51] and α-Syn_{1-6} (α-Syn_{1-17}: $\log K_a$ = 9)[9,10] in equimolar conditions. UV-vis experiments showed that both Eu-DO3A-C3AmpicH and C3AmpicH immediately and completely retrieved $A\beta_{1-16}$-bound Cu^{II} (Fig. 5B and S26, S27). On the other hand, $A\beta_{1-16}$ failed to remove Cu^{II} from Eu^{III}-DO3A-C3AmpicH and C3AmpicH, even when present in a 10-fold excess, indicating that these compounds have stronger affinity for Cu^{II} compared to $A\beta_{1-16}$. As the d–d band of Cu^{II}-α-Syn_{1-6} at 625 nm is too close to the one of the studied Cu ^{II}-complexes, the Cu^{II} transfer between Eu^{III}-DO3A-C3AmpicH and α-Syn_{1-6} was investigated by Eu^{III} luminescence (Fig. 5C and S28) and the stronger affinity of Eu^{III}-DO3A-C3AmpicH compared to α-Syn_{1-6} for Cu^{II} was confirmed.

To conclude, the affinities of Eu-DO3A-C3AmpicH and C3AmpicH for Cu^{II} are very similar, in contrast to the distinct affinities previously observed for Eu-DO3A-pyrGH *vs.* pyrGH. Hence, the propyl linker ensures an effective spatial separation between the Ln^{III} and Cu^{II} complexes, and thereby reduces efficiently the electrostatic repulsion and steric hindrance

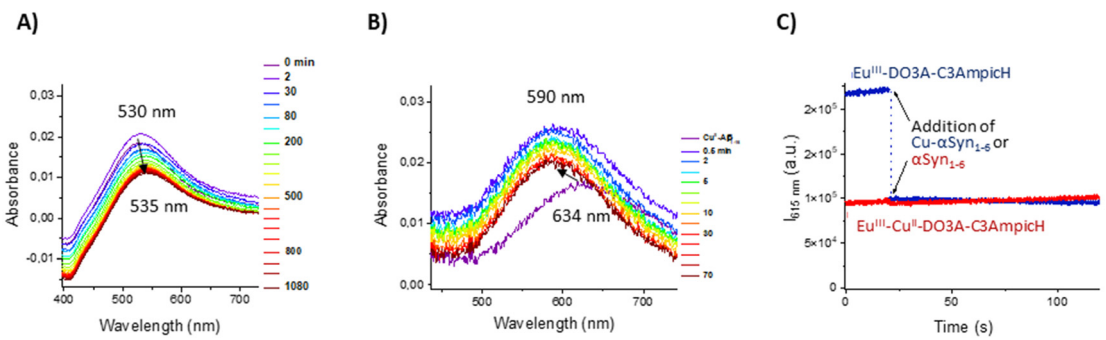

Fig. 5 Competition experiments with HSA, $A\beta_{1-16}$ and α-Syn_{1-6} for Cu^{II}-binding. (A) Competition between Cu^{II}-HSA and Eu^{III}-DO3A-C3AmpicH (1 : 1) monitored *via* the d–d absorption band of Cu^{II}. Conditions: 200 μM Eu^{III}-DO3A-C3AmpicH, 200 μM HSA, 180 μM $CuCl_2$, 50 mM HEPES pH 7.4. (B) Competition between Cu^{II}-$A\beta_{1-16}$ and Eu^{III}-DO3A-C3AmpicH (1 : 1) monitored *via* the d–d absorption band of Cu^{II}. Conditions: 200 μM Eu^{III}-DO3A-C3AmpicH, 200 μM $A\beta_{1-16}$, 180 μM $CuCl_2$, 50 mM HEPES pH 7.4. (C) Competition between α-Syn_{1-6} and Eu^{III}-DO3A-C3AmpicH for Cu^{II}, monitored *via* the Eu^{III}-luminescence intensity at 615 nm. Conditions: 40 μM Eu^{III}-DO3A-C3AmpicH, 40 μM α-Syn_{1-6}, 36 μM $CuCl_2$, 25 mM HEPES pH 7.4, λ_{ex} = 277 nm.

between the two metal centers. The affinity of Eu-DO3A-C3AmpicH and C3AmpicH for Cu^{II} is between those of HSA and $A\beta_{1-16}$, *i.e.* around $\log K_a \sim 11–12$, which corresponds to a dissociation constant in the picomolar range (1–10 pM).

2.6 Study of the Cu^{II}-selectivity

The selectivity of Eu^{III}-DO3A-C3AmpicH and C3AmpicH for Cu^{II} over various metal ions was investigated by UV-Vis absorption and luminescence spectroscopy (Fig. S29–S32). In these experiments, 1 eq. Cu^{II} and 10 eq. Zn^{II} were added to Eu^{III}-DO3A-C3AmpicH and C3AmpicH in different orders. The addition of 10 eq. Zn^{II} caused no change in the d–d transition region but led to a change in the absorption pattern below 300 nm (Fig. 6 and S29B), suggesting that Zn^{II} interacts with the ligand. However, whatever the order of addition of the two metal ions, the Cu^{II}-complex was entirely formed.

The selectivity of Eu^{III}-DO3A-C3AmpicH for Cu^{II} over up to 500 eq. of Zn^{II} was followed by luminescence spectroscopy. The addition of up to 5 eq. Zn^{II} did not significantly impact the luminescence intensity of Eu^{III}-DO3A-C3AmpicH. However, adding 10 or more equivalents resulted in an increase of up to 130% of the initial luminescence (Fig. S29A). This confirms some interactions between Eu^{III}-DO3A-C3AmpicH and Zn^{II} ions. Similar luminescence enhancements have been reported in the literature and are often attributed to an increase in rigidity of the complex upon Zn^{II} binding.[52–54] Another possibility is that Zn^{II} induces conformational changes, bringing the pyridine sensitizer closer to Eu^{III}, enhancing luminescence. The luminescence intensity remained high with the addition of up to 500 eq. of Zn^{II}. With subsequent addition of Cu^{II}, the luminescence immediately decreased, confirming the selectivity for Cu^{II} over Zn^{II}. Similar results were obtained in the presence of 65 eq. of Ca^{II}, 60 eq. of Mg^{II}, 1 eq. of Mn^{II} or Fe^{III} (Fig. S30 and S31), confirming the selectivity of Eu-DO3A-C3AmpicH and C3AmPicH for Cu^{II} in these conditions.

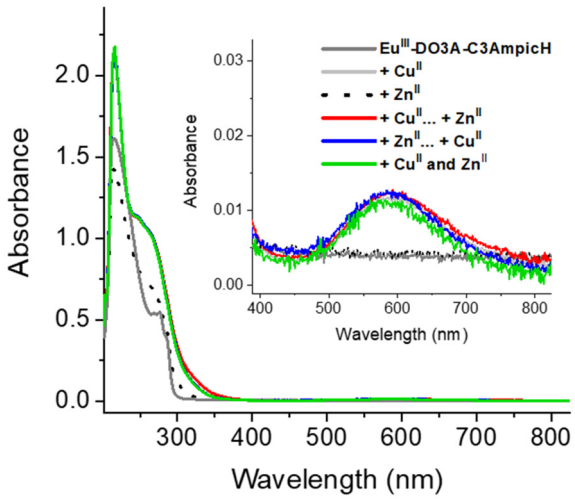

Fig. 6 UV-Vis spectrum of the addition of 1 eq. Cu^{II} and 10 eq. Zn^{II} to Eu^{III}-DO3A-C3AmpicH, conditions: 100 μM Eu^{III}-DO3A-C3AmpicH, 100 μM $CuCl_2$, 1 mM $ZnSO_4$, 10 mM TRIS pH 7.4.

In order to take into consideration that Cu^{II} is bound to a carrier in the body, competition experiments were also carried out in the presence of $A\beta_{1-16}$. Thus, Cu^{II} and Zn^{II} were added simultaneously to a solution containing Eu^{III}-DO3A-C3AmpicH and $A\beta_{1-16}$, in equimolar concentrations (Fig. S32). Given that $A\beta_{1-16}$ has a 10^4-fold stronger affinity for Cu^{II} over Zn^{II}, this experimental set-up represents more challenging conditions compared to the experiments in the absence of $A\beta_{1-16}$. Immediately after the addition of Cu^{II} and Zn^{II}, a d–d band centered at 600 nm emerged and showed no further temporal evolution in terms of intensity or position. The d–d band maximum was red-shifted by about 5 nm compared to Eu^{III}–Cu^{II}-DO3A-C3AmpicH, suggesting that a minor part of Cu^{II} remains bound to $A\beta_{1-16}$, whose absorption maximum lies around 635 nm when complexed to Cu^{II}.

3. Conclusion

The Ln^{III}-DO3A-C3AmpicH complex was developed to bind Cu^{II}, and increase the distance between the Ln^{III}- and Cu^{II}-binding sites in order to achieve a desirable affinity for Cu^{II}. Such design was successful as the Cu^{II} affinity of Cu^{II}-C3AmpicH and Eu^{III}–Cu^{II}-DO3A-C3AmpicH are very similar, and in the appropriate range to compete with the $A\beta_{1-16}$ peptide, or α-Synuclein. The selectivity for Cu^{II} *vs.* other physiological cations, particularly Zn^{II}, is very good. Cu^{II} could be detected by following the quenching of the luminescence of Eu-DO3A-C3AmpicH. This complex is able to detect Cu^{II} bound to Aβ or α-synuclein, key Cu^{II} reservoirs in Alzheimer's and Parkinson's diseases respectively, by luminescence. However, no change of relaxivities is observed upon Cu^{II} addition due to the absence of binding of the amide group to the Ln^{III} in the absence of Cu^{II}, in contrast to what has been observed in the literature. This is due to the steric hindrance brought by the relatively rigid Cu^{II} binding site, as demonstrated by DFT calculations. Current efforts are pursued to further modify the Cu^{II}-binding site in order to obtain a relaxivity response.

Author contributions

K. Z. performed synthesis of DO3A-C3AmpicH and C3AmpicH, Cu-binding studies, selectivity studies and contributed to analysis and writing. B. V. performed measurements, analysis and writing of EPR part; A. P. performed the relaxometric measurements, C. P.-I. performed DFT calculations and contributed to writing, P. F. supervised physico-chemical work and contributed to writing, C. B. supervised relaxometric measurements, did analysis and contributed to writing, A. S. supervised synthetic work and contributed to writing.

Conflicts of interest

The authors declare no conflict of interest.

Data availability

Data supporting this study are included within the supplementary information (SI). Supplementary information is available. See DOI: https://doi.org/10.1039/d5dt01735a.

Acknowledgements

The French Ministry of Education and Research is acknowledged for a Ph.D. fellowship to Z. K. We also thank for the financial support from the Agence Nationale de la Recherche (SteRIC ANR-22-CE07-0030).

References

1 R. A. Festa and D. J. Thiele, *Curr. Biol.*, 2011, **21**, R877–R883.
2 L. Chen, J. Min and F. Wang, *Signal Transduction Targeted Ther.*, 2022, **7**, 1–16.
3 N. E. Hellman and J. D. Gitlin, *Annu. Rev. Nutr.*, 2003, **22**, 439–458.
4 K. Bossak-Ahmad, T. Frączyk, W. Bal and S. C. Drew, *ChemBioChem*, 2020, **21**, 331–334.
5 S. Catalani, M. Paganelli, M. E. Gilberti, L. Rozzini, F. Lanfranchi, A. Padovani and P. Apostoli, *J. Trace Elem. Med. Biol.*, 2018, **45**, 176–180.
6 V. Borghesani, B. Alies and C. Hureau, *Eur. J. Inorg. Chem.*, 2018, **2018**, 1–1.
7 P. Faller and C. Hureau, *Dalton Trans.*, 2009, 1080–1094.
8 S. Bucossi, M. Ventriglia, V. Panetta, C. Salustri, P. Pasqualetti, S. Mariani, M. Siotto, P. M. Rossini and R. Squitti, *J. Alzheimer's Dis.*, 2011, **24**, 175–185.
9 R. De Ricco, D. Valensin, S. Dell'acqua, L. Casella, C. Hureau and P. Faller, *ChemBioChem*, 2015, **16**, 2319–2328.
10 T. Kowalik-Jankowska, A. Rajewska, K. Wiśniewska, Z. Grzonka and J. Jezierska, *J. Inorg. Biochem.*, 2005, **99**, 2282–2291.
11 D. Valensin, F. Camponeschi, M. Luczkowski, M. C. Baratto, M. Remelli, G. Valensin and H. Kozlowski, *Metallomics*, 2011, **3**, 292–302.
12 A. Poujois, J. Poupon and F. Woimant, in *Clinical and Translational Perspectives on WILSON DISEASE*, ed. N. Kerkar and E. A. Roberts, Academic Press, 2019, pp. 249–255.
13 R. Squitti, R. Ghidoni, I. Simonelli, I. D. Ivanova, N. A. Colabufo, M. Zuin, L. Benussi, G. Binetti, E. Cassetta, M. Rongioletti and M. Siotto, *J. Trace Elem. Med. Biol.*, 2018, **45**, 181–188.
14 S. El Balkhi, J. M. Trocello, J. Poupon, P. Chappuis, F. Massicot, N. Girardot-Tinant and F. Woimant, *Clin. Chim. Acta*, 2011, **412**, 2254–2260.
15 E. Falcone, M. Okafor, N. Vitale, L. Raibaut, A. Sour and P. Faller, *Coord. Chem. Rev.*, 2021, **433**, 213727.
16 K. P. Malikidogo, H. Martin and C. S. Bonnet, *Pharmaceuticals*, 2020, **13**, 436.
17 J. Wahsner, E. M. Gale, A. Rodríguez-Rodríguez and P. Caravan, *Chem. Rev.*, 2019, **119**, 957–1057.
18 É. Tóth, L. Helm and A. E. Merbach, *Contrast Agents I. Topics in Current Chemistry*, Springer, Berlin, Heidelberg, 221st edn, 2002.
19 A. Merbach, L. Helm and É. Tóth, *The Chemistry of Contrast Agents in Medical Magnetic Resonance Imaging*, John Wiley and Sons, 2nd edn, 2013.
20 P. Yue, T. Nagendraraj, G. Wang, Z. Jin and G. Angelovski, *Chem. Sci.*, 2024, **15**, 20122–20154.
21 E. L. Que and C. J. Chang, *Chem. Soc. Rev.*, 2009, **39**, 51–60.
22 V. C. Pierre, S. M. Harris and S. L. Pailloux, *Acc. Chem. Res.*, 2018, **51**, 342–351.
23 P. Caravan, *Chem. Soc. Rev.*, 2006, **35**, 512–523.
24 M. C. Heffern, L. M. Matosziuk and T. J. Meade, *Chem. Rev.*, 2014, **114**, 4496–4539.
25 J. P. C. Coverdale, J. P. Barnett, A. H. Adamu, E. J. Griffiths, A. J. Stewart and C. A. Blindauer, *Metallomics*, 2019, **11**, 1805–1819.
26 W. Bal, M. Sokołowska, E. Kurowska and P. Faller, *Biochim. Biophys. Acta*, 2013, **1830**, 5444–5455.
27 A. I. Bush, W. H. Pettingell, G. Multhaup, M. D. Paradis, J. P. Vonsattel, J. F. Gusella, K. Beyreuther, C. L. Masters and R. E. Tanzi, *Science*, 1994, **265**, 1464–1467.
28 E. L. Que and C. J. Chang, *J. Am. Chem. Soc.*, 2006, **128**, 15942–15943.
29 N. N. Paranawithana, A. F. Martins, V. Clavijo Jordan, P. Zhao, S. Chirayil, G. Meloni and A. D. Sherry, *J. Am. Chem. Soc.*, 2019, **141**, 11009–11018.
30 K. Zimmeter, A. Pallier, B. Vileno, M. Sanadar, F. Szeremeta, C. Platas-Iglesias, P. Faller, C. S. Bonnet and A. Sour, *Inorg. Chem.*, 2024, **63**, 23067–23076.
31 M. Sanadar, K. Zimmeter, H. Martin, A. Pallier, B. Vileno, P. Faller, A. Sour and C. S. Bonnet, *Eur. J. Inorg. Chem.*, 2025, **28**, e202500049.
32 K. Zimmeter, B. Vileno, C. Platas-Iglesias, B. Vinjamuri, A. Sour and P. Faller, *Inorg. Chem.*, 2023, **62**, 9429–9439.
33 A. Mishra, N. K. Logothetis and D. Parker, *Chem. – Eur. J.*, 2011, **17**, 1529–1537.
34 M. Regueiro-Figueroa, S. Gündüz, V. Patinec, N. K. Logothetis, D. Esteban-Gómez, R. Tripier, G. Angelovski and C. Platas-Iglesias, *Inorg. Chem.*, 2015, **54**, 10342–10350.
35 P. Kadjane, C. Platas-Iglesias, P. Boehm-Sturm, V. Truffault, G. E. Hagberg, M. Hoehn, N. K. Logothetis and G. Angelovski, *Chem. – Eur. J.*, 2014, **20**, 7351–7362.
36 A. Congreve, D. Parker, E. Gianolio and M. Botta, *Dalton Trans.*, 2004, 1441–1445.
37 F. Oukhatar, H. Meudal, C. Landon, N. K. Logothetis, C. Platas-Iglesias, G. Angelovski and É. Tóth, *Chem. – Eur. J.*, 2015, **21**, 11226–11237.
38 M. Regueiro-Figueroa, S. Gündüz, V. Patinec, N. K. Logothetis, D. Esteban-Gómez, R. Tripier,

G. Angelovski and C. Platas-Iglesias, *Inorg. Chem.*, 2015, **54**, 10342–10350.
39 S. Laine, J. F. Morfin, M. Galibert, V. Aucagne, C. S. Bonnet and É. Tóth, *Molecules*, 2021, **26**, 2176.
40 C. Harford and B. Sarkar, *Acc. Chem. Res.*, 1997, **30**, 123–130.
41 D. M. Rudkevich, W. Verboom, E. van der Tol, C. J. Van Staveren, F. M. Kaspersen, J. W. Verhoeven and D. N. Reinhoudt, *J. Chem. Soc., Perkin Trans. 2*, 1995, 131–134.
42 L. Pellegatti, J. Zhang, B. Drahos, S. Villette, F. Suzenet, G. Guillaumet, S. Petoud and É. Tóth, *Chem. Commun.*, 2008, 6591–6593.
43 É. Tóth, O. M. N. Dhubhghaill, G. Besson, L. Helm and A. E. Merbach, *Magn. Reson. Chem.*, 1999, **37**, 701–708.
44 K. A. Brameld, B. Kuhn, D. C. Reuter and M. Stahl, *J. Chem. Inf. Model.*, 2008, **48**, 1–24.
45 H. Sigel and R. B. Martin, *Chem. Rev.*, 1982, **82**, 385–426.
46 A. Belczyk-Ciesielska, I. A. Zawisza, M. Mital, A. Bonna and W. Bal, *Inorg. Chem.*, 2014, **53**, 4639–4646.
47 A. W. Addison and E. Sinn, *Inorg. Chem.*, 1983, **22**, 1225–1228.
48 J. Peisach and W. E. Blumberg, *Arch. Biochem. Biophys.*, 1974, **165**, 691–708.
49 M. Drosou, C. A. Mitsopoulou, M. Orio and D. A. Pantazis, *Magnetochemistry*, 2022, **8**, 36.
50 G. Sciortino, G. Lubinu, J.-D. Maréchal and E. Garribba, *Magnetochemistry*, 2018, **4**, 55.
51 V. Borghesani, B. Alies and C. Hureau, *Eur. J. Inorg. Chem.*, 2018, **2018**, 1–1.
52 K. C. Weerasinghe and L. Wang, *ChemRxiv*, 2023, preprint, DOI: **10.26434/CHEMRXIV-2023-PJG54-V2**.
53 S. A. McFarland and N. S. Finney, *J. Am. Chem. Soc.*, 2002, **124**, 1178–1179.
54 J. Luo, W. S. Li, P. Xu, L. Y. Zhang and Z. N. Chen, *Inorg. Chem.*, 2012, **51**, 9508–9516.